Catalysis Science & Technology

PAPER

View Article Online
View Journal | View Issue

Cite this: *Catal. Sci. Technol.*, 2014, 4, 3141

Oxidative esterification of ethylene glycol in methanol to form methyl glycolate over supported Au catalysts†

Yi-Hu Ke, Xiao-Xia Qin, Chun-Ling Liu, Rong-Zhen Yang and Wen-Sheng Dong*

Received 30th April 2014,
Accepted 27th May 2014

DOI: 10.1039/c4cy00556b

www.rsc.org/catalysis

Au/ZnO and Au/Al_2O_3 catalysts with various mean Au particle diameters (2.0–7.4 nm) were prepared by the deposition of pre-formed Au colloids. These catalysts were evaluated in the oxidative esterification of ethylene glycol to methyl glycolate. The results show that the catalytic activity per surface Au atom is independent of Au particle diameter in the range of 3–7.4 nm, whereas smaller Au particles (~2.0 nm) show an inferior activity. This behavior was observed on both Au/ZnO and Au/Al_2O_3 catalysts. This observed correlation between activity and Au particle diameter confirms the assertion that only exposed atoms are catalytically active. We prepared gold nanoparticles with a uniform mean diameter of ~3 nm loaded on various supports, *i.e.* ZnO, Al_2O_3, SiO_2, TiO_2 and CeO_2. Among these five catalysts, Au/ZnO gave the best catalytic activity in the reaction followed by Au/Al_2O_3. Au/SiO_2, Au/TiO_2 and Au/CeO_2 gave significantly lower activities. The variation in catalytic behavior of these gold catalysts on different supports originates from differences in the anchoring of the supported Au particles, the gold oxidation state, the gold–support interaction, and the acidity of the support.

1. Introduction

Many methyl esters are industrially important chemicals, which can be used as solvents, extractants, diluents, and intermediates or as products in the perfume industry.[1] The conventional route for the production of methyl esters involves a two-step synthetic procedure in which the synthesis of carboxylic acids or activated carboxylic acid derivatives such as acid anhydrides or chlorides is first required.[2,3] The direct formation of methyl esters from the oxidation of primary alcohols in methanol is also well known. However, these methods generally employ stoichiometric oxidants such as iodine, trichloroisocyanuric acid, (diacetoxy)-iodobenzene or hypochlorite reagents.[4–6] Hence, the use of facile, cost-effective, and environmentally friendly procedures with air as the oxidant together with heterogeneous catalysts will avoid the use of erosive acid catalysts and a large excess of reagents. This has attracted substantial interest.

The oxidative esterification of ethylene glycol to methyl glycolate using air as the oxidant over heterogeneous Au catalysts was first reported by Hayashi *et al.* from the Nippon Shokubai company.[7] This route represents significant progress towards a greener commercial process for the clean and efficient production of carboxylic esters. Since then, the oxidative esterification of various alcohols, *e.g.* primary alcohols, aromatic and aliphatic primary alcohols, 1,2-propanediol, glycerol, *etc.* or aldehydes has been reported by several research groups.[8–14] Au catalysts supported on various supports, *e.g.* β-Ga_2O_3, TiO_2, CeO_2, and Fe_2O_3, have been found to exhibit catalytic activity in the process. Although a previous study found that β-Ga_2O_3 containing increased acid sites was much more active and selective than conventional oxide-supported Au catalysts,[8] the exact nature of the support effect still needs to be explored further, because a deep understanding of the role of the support may lead to significant improvements in supported Au catalysts for the oxidative esterification of alcohols.

Supported Au nanoparticles have shown unique catalytic properties in a variety of reactions such as CO oxidation, the aerobic oxidation of alcohols, propylene epoxidation, hydrogen peroxide synthesis, hydrogenation reactions, C–C coupling reactions, *etc.*[15–17] It is generally accepted that the catalytic behavior of Au depends to a large extent on the size of the Au particles and the nature of the support, although many other issues such as the Au–support interaction, the Au particle shape and the chemical state of Au may also affect the catalytic performance. For example, for the oxidation of CO it has been shown both experimentally and theoretically that the activity of Au particles increases with a decrease in the particle size and the activity is strongly affected by the

Key Laboratory of Applied Surface and Colloid Chemistry (SNNU), MOE, School of Chemistry and Chemical Engineering, Shaanxi Normal University, Xi'an 710062, China. E-mail: wsdong@snnu.edu.cn; Fax: +86 029 81530806; Tel: +86 029 81530806

† Electronic supplementary information (ESI) available. See DOI: 10.1039/c4cy00556b

support.[18–23] However, for the gas-phase non-oxidative dehydrogenation of ethanol, Hensen *et al.* found that gold nanoparticles of about 6 nm showed a much higher activity than smaller or larger particles. However, in the presence of oxygen the intrinsic activity was constant at up to about 7 nm, and it increased for larger particles.[24] For liquid oxidation reactions, the situation is even more complicated.[25–36] A volcano-type relationship between gold particles and their activity towards selective ethanol oxidation to acetic acid in an aqueous solution was reported by Xu *et al.* They observed that, among 3–30 nm Au particles, Au particles with an average diameter of 5 nm showed an activity about 3 times higher than that of smaller (~3 nm) Au particles and 15 times higher than that of larger (10–30 nm) Au particles.[25] In the selective liquid phase oxidation of glycols, Bianchi *et al.* found that the activity of Au catalysts supported on oxides (Al_2O_3, TiO_2) increased upon a decrease in the Au particle diameter from 7.2 to 3.7 nm. However, on carbon the maximum activity was achieved for gold particles with a mean diameter of around 7–8 nm.[26] For the aerobic oxidation of benzyl alcohol, Haider *et al.* found optimal activity for CeO_2 and TiO_2 supported Au catalysts with a medium particle size (*ca.* 6.9 nm), whereas smaller and bigger particles showed inferior activity.[27] For the oxidation of glucose, Comotti *et al.* found that the catalytic activity was inversely proportional to the diameter of colloidal Au particles in the range of 3–6 nm.[33] These results indicate that an Au size effect is apparent in different reactions. An understanding of the effect of Au particle size and the function of the supports in various Au-catalyzed reactions will assist in designing highly efficient Au catalysts.

To understand the particle size and support effects, it is crucial that only one preparation method is used, as important variables such as impurities, residues on the catalyst surface, and particle morphology might be altered when using different preparation techniques.[27] Hence, in this work gold nanoparticles with different average diameters were prepared using polyvinyl alcohol as a protecting agent and $NaBH_4$ as a reductant and only the reaction temperature was changed. The Au particles were deposited onto the ZnO and Al_2O_3 supports by the colloidal deposition method to determine the Au size effect. The Au catalysts were supported on five different supports, ZnO, Al_2O_3, SiO_2, TiO_2, and CeO_2, with a similar gold particle size to investigate the effect of the support. From a combined study of these effects, we identified important structural features of the gold particle size and the support that control the efficiency of the gold catalysts in the oxidative esterification of ethylene glycol.

2. Experimental

2.1 Catalyst preparation

The commercially available powder supports γ-Al_2O_3 and SiO_2 were purchased from Sinopharm Chemical Reagent Co. Ltd. (Shanghai, China). TiO_2 was P25 from Evonik Industries. ZnO and CeO_2 were prepared by the precipitation method using the corresponding nitrates $Zn(NO_3)_2{\cdot}6H_2O$ and $Ce(NO_3)_3{\cdot}6H_2O$, respectively. The precipitation was carried out by adding sodium carbonate (0.25 M) to the $Zn(NO_3)_2{\cdot}6H_2O$ (0.3 M, 82 mL) solution and an ammonia solution (25%) to the $Ce(NO_3)_3{\cdot}6H_2O$ solution (0.3 M, 39 mL) at 70 °C under vigorous stirring until the pH of the mixture was 8. The obtained solution was then left at 70 °C while stirring for 90 min. The resulting precipitates were filtered, washed with distilled water, dried at 110 °C overnight, and subsequently calcined at 350 °C in air for 4 h.

The colloidal deposition method used in this study has been extensively described elsewhere.[21,37,38] Gold nanoparticles with different average diameters were prepared by the reduction of $HAuCl_4$ (Sinopharm Chemicals (99.99%)) in aqueous solution using polyvinyl alcohol (PVA, Mw 10 000 from Aldrich, 80% hydrolyzed) as a protecting agent and $NaBH_4$ (Sinopharm Chemicals) as a reductant at different temperatures. In a typical preparation, the protecting agent was added (Au/PVA = 2 : 1 mg mg^{-1}) to a 200 mg L^{-1} aqueous gold solution at room temperature (25 °C) under vigorous stirring, followed by a rapid injection of a 0.1 M aqueous solution of $NaBH_4$ (Au/$NaBH_4$ = 1 : 4 mol mol^{-1}) that led to the formation of a dark-orange–brown solution, indicating the formation of gold colloids.

The immobilization of Au particles on the supports, *i.e.* ZnO, Al_2O_3, TiO_2, CeO_2, was accomplished at room temperature (25 °C) by adding these supports to the colloidal gold solution while stirring and they were kept in contact until total adsorption (1.3 wt% gold on the support) occurred, as indicated by the decolorization of the solution. Owing to the different interactions between the metal-oxide particles and the gold nanoparticles, it took 2 to 24 h for the full deposition of gold colloids onto these supports. For ZnO and TiO_2, it took ~2 h. For Al_2O_3, CeO_2, and SiO_2, it required ~24 h. In the case of SiO_2, the pH of the colloidal solution needed to be adjusted to 0.5 with nitric acid during the deposition.[25] The solids were collected by filtration followed by washing the solid with 2 L of doubly-distilled water to remove all the dissolved species (*e.g.* Na^+, Cl^-). Finally, the solids were dried under vacuum at 100 °C for 12 h.

2.2 Catalyst characterization

The crystal structures of the as-prepared samples were characterized by powder X-ray diffraction (XRD) using a Rigaku D/MAX-III X-ray diffractometer (35 kV, 40 mA) with a CuKα source. The diffraction patterns were obtained between 10 and 80° at a scan rate of 8° min^{-1}. The specific surface areas and the pore size distribution of the samples were obtained by N_2 (−196.2 °C) adsorption measurements using a Micromeritics ASAP 2020M system. Before the measurement, the samples were outgassed at 300 °C for 6 h. The surface area (S_{BET}) was calculated using the BET method. The micropore surface area S_{mi} was obtained using the *t*-plot method. The mesoporous surface area (S_{meso}) was determined by subtracting S_{mi} from S_{BET}. The pore size distribution was derived from the desorption branch of the N_2 isotherms using the BJH method.

The total pore volumes (V_p) were estimated considering nitrogen uptake at a relative pressure (P/P_0) of *ca.* 0.99. The average pore diameter (D_p) was estimated from the surface area and the total pore volume ($D_p = 4V_p/S_{BET}$). The crystalline size and microstructure were characterized by transmission electron microscopy (TEM, JEOL JEM-2100). The operating voltage was 200 kV. The particle sizes and distribution of the gold particles were obtained from TEM images by averaging a minimum of 200 particles. By assuming a spherical model for the Au nanoparticles, the dispersion of Au (D) was roughly estimated by the following relationship, $D = 1.17/d$ (nm) × 100%.[28] X-ray photoelectron spectroscopy (XPS) measurements were performed on a PE PHI-5400 spectrometer with an Al Kα source (1486.6 eV). The binding energy was calibrated relative to the C1s peak (285.0 eV) of the contaminant carbon. The accuracy of the BE values was ±0.1 eV. The high-resolution scans were performed over the 78–96 eV (Au 4f spectrum) for the tested samples. The peak area was estimated by calculating the integral of each peak after subtracting an S-shaped background and fitting the experimental peak to a combination of Lorentzian/Gaussian lines of variable proportions. The Au content was determined using an inductively coupled plasma atomic emission spectrometer (ICP-AES, model Atom Scan 16, TJA Corp.).

H_2 temperature programmed reduction (H_2-TPR) experiments were carried out using a Micromeritics AutoChem II-2920 instrument. In each trial, about 50 mg of sample was loaded into a quartz reactor. TPR measurements were performed using 10% hydrogen in argon (30 ml min^{-1}) at a heating rate of 10 °C min^{-1} from room temperature to 900 °C. Hydrogen consumption was monitored online using a thermal conductivity detector.

The acidities of the samples were determined by ammonia temperature-programmed desorption (NH_3-TPD) using a Micromeritics AutoChemII-2920 system. A 100 mg sample was loaded into a sample tube and pretreated in He at 200 °C for 60 min. The sample was cooled, and NH_3 was adsorbed at 120 °C for 30 min, and then the sample was further purged with dry helium at the same temperature to remove weakly adsorbed NH_3. Finally, the sample was heated at a linear rate of 10 °C min^{-1} under dry helium (30 ml min^{-1}) up to 700 °C. The effluent was monitored by a quadrupole mass spectrometer.

2.3 Reaction and analysis

All the reactions were conducted in a 35 mL stainless steel autoclave equipped with a magnetic stirrer. In a typical experiment, 0.9 g of catalyst, 17.4 g of methanol and 3.43 g of ethylene glycol were added to the autoclave. The autoclave was then sealed tightly, purged and pressurized to 3.0 MPa with O_2 at room temperature. The reaction proceeded at 100 °C for 20 min. After the reaction, the reactor was cooled to less than 5 °C with an ice–water mixture and depressurized. An internal standard of *n*-amyl alcohol was added to the liquid products. Quantitative analysis was performed using an Agilent 6820 GC with an INNOWAX capillary column (30 m × 0.32 mm × 0.5 μm) and an FID.

The conversion of ethylene glycol (EG) was calculated based on the following equation:

$$\text{EG conversion (\%)} = \frac{\text{moles of converted EG}}{\text{moles of initial EG}} \times 100\%$$

The selectivity of methyl glycolate (MGC) was calculated based on the following equation:

$$\text{MGC selectivity (\%)} = \frac{\text{moles of MGC formed}}{\text{moles of converted EG}} \times 100\%$$

3. Results

3.1 Characterization of the supports

The surface area, pore volume and average pore diameters of the five supports are shown in Table 1. XRD patterns of the ZnO, Al_2O_3, SiO_2 and TiO_2 supports in Fig. S1 (ESI†) show well-crystallized diffraction peaks while the diffraction peaks of CeO_2 are not sharp, indicating that this support is not well crystallized.

3.2 Au particle size effect

Four different sizes of Au colloids were prepared by the reduction of $HAuCl_4$ in aqueous solution using polyvinyl alcohol as a protecting agent and $NaBH_4$ as a reductant. We found that the reaction temperature was an important factor in controlling the reduction rate of metal cations, and higher temperatures gave a larger mean particle size. The reduction of $HAuCl_4$ in aqueous solution gave 1.8 nm Au particles at 0 °C, 2.9 nm at 25 °C, 4.8 nm at 60 °C, and 7.4 nm at 90 °C (see Fig. S2, ESI†). The Au particles in Fig. S2a–c (ESI†) have a near-spherical shape with a homogeneous size distribution, whereas the Au particles prepared at 90 °C (Fig. S2d, ESI†) have an oval shape with a broad size distribution.

The immobilization of these Au colloids onto the ZnO support was also studied by HRTEM to verify the sizes of the Au particles after immobilization. Typical TEM micrographs and the corresponding Au particle size distributions for the Au/ZnO catalysts with different mean Au particle sizes are shown in Fig. 1. It is clear that after immobilization, only minor amounts of agglomerated particles were detected and the determination of mean particle size gave similar values to those obtained for the Au colloids in solution.

Table 2 shows the dependence of catalytic performance on the mean size of the Au nanoparticles in Au/ZnO. The loading of Au onto these catalysts was consistent (~1.25 wt%). High selectivity towards methyl glycolate (93.1–95.3%) was obtained for all these catalysts, which indicates that the Au particle size did not affect product selectivity. The product selectivity was mainly determined by the nature of the support, which will be explained in section 3.3. Table 2 shows that the conversion of ethylene glycol depends strongly on the mean size of the Au nanoparticles. With a decrease in the

Table 1 The physico-chemical properties of various supports

Supports	S_{BET} ($m^2\ g^{-1}$)	S_{meso} ($m^2\ g^{-1}$)	V_p ($cm^3\ g^{-1}$)	V_{meso} ($cm^3\ g^{-1}$)	D_p (nm)
ZnO	31.8	25.0	0.20	0.197	24.7
γ-Al_2O_3	185.9	88.4	0.16	0.11	5.8
SiO_2	309.8	293.0	0.93	0.922	8.7
TiO_2	48.5	46.3	0.19	0.19	15.9
CeO_2	27.9	23.0	0.11	0.108	16.6

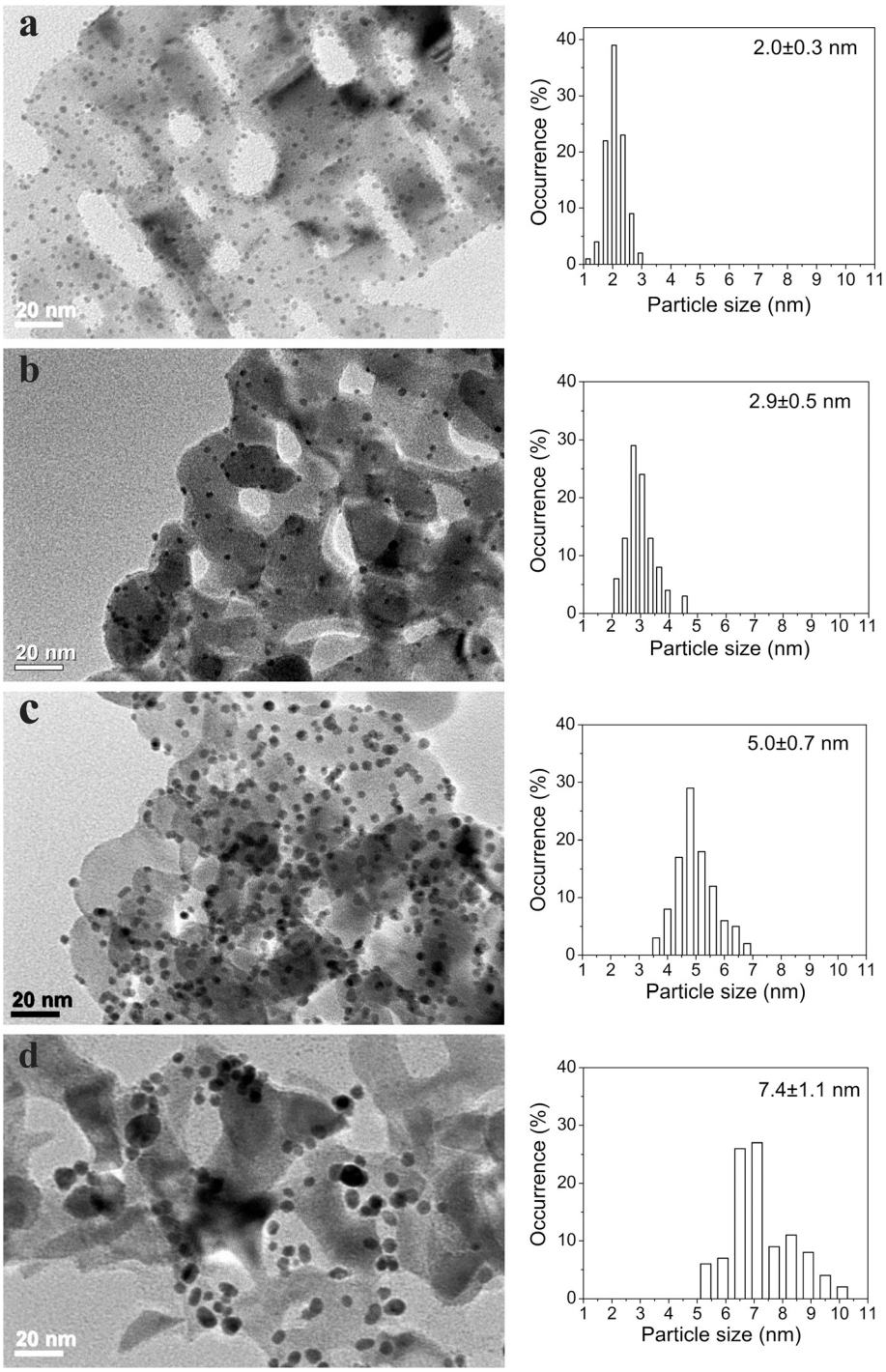

Fig. 1 TEM micrographs and the corresponding Au particle size distributions for Au/ZnO catalysts: a) Au(2.0)/ZnO; b) Au(2.9)/ZnO; c) Au(4.9)/ZnO; d) Au(7.4)/ZnO.

Table 2 Catalytic performance of Au/ZnO catalysts with varying mean Au particle sizes[a]

Catalysts	Au loading (wt%)	Mean Au size (nm)	Au dispersion (%)	EG conversion (%)	MGC selectivity (%)	TOF[b] (s^{-1})
Au(2.0)/ZnO	1.25	2.0	58.5	17.8	93.9	0.245
Au(2.9)/ZnO	1.25	2.9	40.3	21.6	94.8	0.432
Au(4.9)/ZnO	1.26	4.9	23.8	12.3	95.3	0.417
Au(7.4)/ZnO	1.25	7.4	15.8	7.6	93.1	0.388

[a] Reaction conditions: catalyst 0.9 g, methanol 17.4 g, EG = 3.43 g, 3.0 MPa, 100 °C, 20 min. [b] Moles of converted ethylene glycol per mole of surface gold atoms per second.

mean Au particle diameter from 7.4 to 2.9 nm, the conversion of ethylene glycol over the catalysts increased. However, the catalytic activity per surface Au atom is roughly independent of the diameter of the Au particles in the range of 2.9–7.4 nm (TOF: ~0.4 s^{-1}). Au/ZnO with a 2.0 nm mean Au particle diameter had the lowest TOF of 0.245 s^{-1}.

We also prepared four Au/Al_2O_3 catalysts with different Au particle diameters, *i.e.* 2.0, 3.0, 5.0, and 7.6 nm (see Fig. S3, ESI†), and determined their catalytic activities in the oxidative esterification of ethylene glycol to examine whether the Au size effect varies with the support. The same activity change trend was observed (see Table S1, ESI†). The TOF value was ~0.2 s^{-1} for the 2.9–7.4 nm Au particles, which is lower than that of Au/ZnO (~0.4 s^{-1}). The Au/Al_2O_3 catalyst with a 2.0 nm mean Au particle diameter gave the lowest TOF of 0.133 s^{-1}.

To verify whether the oxidative esterification of ethylene glycol catalyzed by Au/ZnO is heterogeneous or homogeneous, we investigated Au leaching during the reaction. The heterogeneous Au(2.9)/ZnO catalyst was filtered while hot after a 30 min reaction (*ca.* 28% ethylene glycol conversion) and the filtrate was allowed to react for a further 1.5 h under the same conditions. The conversion of ethylene glycol was 29% after that time (*i.e.* no change). In addition, ICP analysis confirmed that none of the Au species was detected in the reaction mixtures, confirming that the reaction is heterogeneous.

The recyclability of Au(2.9)/ZnO in the oxidative esterification of ethylene glycol at 100 °C was also examined. As shown in Fig. 2, the conversion of ethylene glycol and the selectivity toward methyl glycolate did not change significantly during three successful cycles. Additionally, we also examined the catalytic performance of the Au(2.9)/ZnO catalyst after storage in a refrigerator for 7 months. We found similar catalytic activity to that of the fresh catalyst. HRTEM observation (not shown) confirmed that this catalyst had a mean Au particle diameter of 3.0 ± 0.51 nm, which is similar to that of the fresh catalyst, confirming that the Au/ZnO catalyst is very stable.

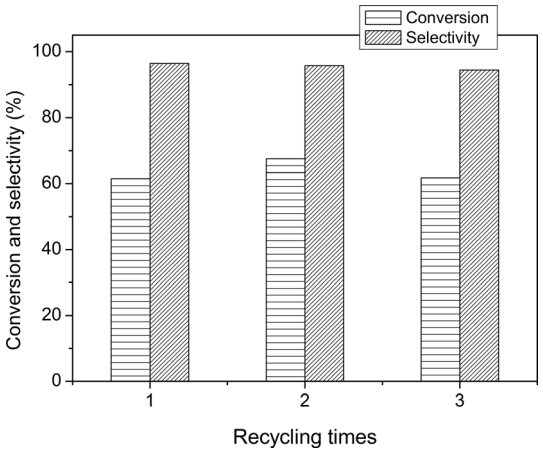

Fig. 2 Recycling of Au(2.9)/ZnO for the oxidative esterification of ethylene glycol (reaction conditions: catalyst 0.9 g, methanol 17.4 g, EG = 3.43 g, 3.0 MPa, 100 °C, 2 h).

3.3 Support effect

A rigorous study into the effect of the support requires the use of catalysts with uniform Au particle sizes. Hence, in this study the supported Au catalysts were prepared by the deposition of Au colloids with a mean particle diameter of 2.9 ± 0.3 nm onto ZnO, Al_2O_3, SiO_2, TiO_2, and CeO_2 supports. The performance of these catalysts in the oxidative esterification of ethylene glycol is shown in Table 3. The activities for the pure supports were also tested before catalyst evaluation and showed that under the conditions used no product was detected. The Au nanoparticles supported on TiO_2 and CeO_2 gave much lower activities with 3.4% and 4.3% ethylene glycol conversion, respectively. The Au/SiO_2 also gave a lower ethylene glycol conversion (12.2%). A medium ethylene glycol conversion (~60.7%) was obtained over the Au/Al_2O_3 catalyst. Among all the supported catalysts, Au(2.9)/ZnO gave the best catalytic activity with 97.4% ethylene glycol conversion. Moreover, Au(2.9)/ZnO gave the highest selectivity towards methyl glycolate followed by Au/Al_2O_3, Au/SiO_2, Au/TiO_2 and Au/CeO_2. The main by-products of the reaction over these supported Au catalysts, as determined by GC-MS, are methyl formate, 1-ethoxyethane-1,2-diol, 1-methoxyethane-1,2-diol, 2,2-dimethoxyethanol, *etc.* Because it is very difficult to obtain pure reagents, the amounts of these by-products were not determined.

Typical TEM micrographs and the corresponding Au particle size distributions for the fresh Au catalysts are shown in Fig. 3. The mean diameters of the Au nanoparticles for all these samples range from 2.9 to 3.3 nm. Fig. S4 (ESI†) shows TEM micrographs and the corresponding Au particle size distributions for these Au catalysts after the reaction. By comparison with fresh Au catalysts, the mean Au particle diameters and distributions of the corresponding used Au catalysts increase to some extent. The mean Au particle

Table 3 Catalytic performance of Au catalysts supported on different supports

Catalysts	Au loading[a] (wt%)	Au size[b] (nm)	EG conversion (%)	MGC selectivity (%)	TOF[c] (s^{-1})
Au(2.9)/ZnO	1.25 (1.26)	2.9 (3.0)	97.4	95.4	—
Au/Al_2O_3	1.35 (1.37)	3.0 (4.4)	60.7	91.7	—
Au/SiO_2	1.15 (1.13)	3.2 (5.0)	12.2	89.7	0.012
Au/TiO_2	1.23 (1.25)	3.3 (5.9)	3.4	56.2	0.003
Au/CeO_2	1.31 (1.33)	3.3 (6.8)	4.3	33.7	0.0037

Reaction conditions: catalyst 0.5 g, methanol 4.83 g, EG = 0.935 g, 3.0 MPa, 100 °C, 4 h.[a] The values in parentheses are Au loading of the used catalysts. [b] The values in parentheses are Au particle sizes of the used catalysts. [c] The moles of converted ethylene glycol per mole of surface gold atoms per second.

diameter for the fresh Au(2.9)/ZnO catalyst was 2.9 ± 0.5 nm. After the reaction, it increased slightly to 3.0 ± 0.8 nm. For Au/Al_2O_3, before the reaction the mean Au particle diameter was 3.0 ± 0.8 nm and after the reaction it increased to 4.4 ± 1.0 nm. For Au/SiO_2, Au/TiO_2, and Au/CeO_2, after the reaction the mean Au particle diameters increased significantly. These results suggest that in this study the anchoring of Au particles strongly depends on the type of support. ZnO has the strongest anchoring effect toward Au particles followed by Al_2O_3, SiO_2, TiO_2 and CeO_2.

Au loading before and after the reaction, as measured by inductively coupled plasma atomic emission spectrometry (ICP-AES), is listed in Table 3. These results confirm that no Au leaching occurred during the reaction.

The surface gold content and the electronic state of the catalysts were characterized by XPS and the results are shown in Table 4 and Fig. 4. The binding energies of Au(0) $4f_{7/2}$ are 83.5, 83.5, and 83.4 eV for Au/TiO_2, Au(2.9)/ZnO, and Au/ZnO-300 (prepared by calcination of Au(2.9)/ZnO at 300 °C in air for 3 h), respectively. These values are lower than that of bulk gold at 84.0 eV, indicating the presence of a gold–support interaction. For Au/SiO_2, the binding energy of Au(0) $4f_{7/2}$ was 84.3 eV, indicating that the interaction between Au and the SiO_2 support is very weak. For Au/Al_2O_3, about 27.5% of the surface gold was in the oxidized state because of the stabilization of Au^+ by Al_2O_3. For Au/CeO_2, about 42.4% of the surface gold was in the oxidized state (Au^{3+}). We also found that Au(2.9)/ZnO had the highest gold surface content (15.5%). Au/ZnO-300 had a lower gold surface content (11.4%) than Au(2.9)/ZnO, which may be due to the growth of gold particles or diffusion into the pores of ZnO during calcination at 300 °C for 3 h. Au/CeO_2 gave a higher surface gold content than Au/Al_2O_3, Au/SiO_2, and Au/TiO_2. TEM confirmed that the Au catalysts that were supported on these five different supports had similar Au particle sizes (2.9–3.3 nm); hence, the lower surface gold content in Au/SiO_2 and Au/TiO_2 may suggest that most of the Au particles in these two catalysts entered the pores of the supports, which could not be detected by XPS analysis.

H_2 temperature programmed reduction curves for the Au catalysts, ZnO, and CeO_2 are shown in Fig. 5. No H_2 consumption peaks were observed for both Au/TiO_2 and Au/SiO_2, indicating that Au was present in the metallic state. These results are consistent with the XPS analysis. ZnO did not have a reduction peak below 900 °C. Au/ZnO had two small reduction peaks at 450 and 575 °C. Au/ZnO-300 had a similar reduction pattern to that of Au/ZnO, but the peak areas were slightly smaller. XPS analysis confirmed that the Au in these two Au/ZnO samples was in the metallic state, and hence the peaks came from the reduction of lattice oxygen in the catalyst. These results suggest the presence of a strong interaction between gold and ZnO. Gold may increase the oxygen mobility and lattice oxygen accessibility of ZnO, and as a result, the reduction temperature of ZnO would decrease. Previously, Muhler *et al.* also found that the presence of Au particles enhanced the number of exposed oxygen vacancies in ZnO, presumably located at the interface region in Au/ZnO.[39]

Au/Al_2O_3 had a small reduction peak at 400 °C with a main reduction peak at 500 °C, which could be attributed to the reduction of Au^+ species. CeO_2 had a small reduction peak around 600 °C and a large peak above 850 °C, which could be attributed to the reduction of the surface shell and bulk CeO_2, respectively.[40] Au/CeO_2 had four reduction peaks around 120, 300, 500, and 750 °C. The peak at 120 °C may be related to the reduction of Au^{3+} to Au^+ while the peak at 300 °C could be assigned to the reduction of Au^+ to Au^0. By comparison with CeO_2, the peaks attributed to the reduction of the surface shell and bulk of the support in Au/CeO_2 shifted to 500 and 750 °C, respectively. This may be due to the presence of a H_2 spillover effect on the Au/CeO_2.

Temperature programmed desorption (TPD) of NH_3 over these Au catalysts was conducted to examine the acid properties of the catalysts and the results are shown in Fig. 6. As shown in Fig. 6, the desorption of NH_3 was examined for Au/Al_2O_3 and Au(2.9)/ZnO, and we found that these two catalysts contained acidic sites. From the temperature and intensity of the NH_3 desorption peak, we found that Au(2.9)/ZnO was more strongly acidic although the total amount of acid was lower than that in Au/Al_2O_3. On the other hand, no desorption of NH_3 was detected from Au/SiO_2, Au/TiO_2 and Au/CeO_2, indicating that these catalysts have no significant acidity.

4. Discussion

This study confirms that the catalytic activity per surface Au atom (TOF) in the oxidative esterification of ethylene glycol is

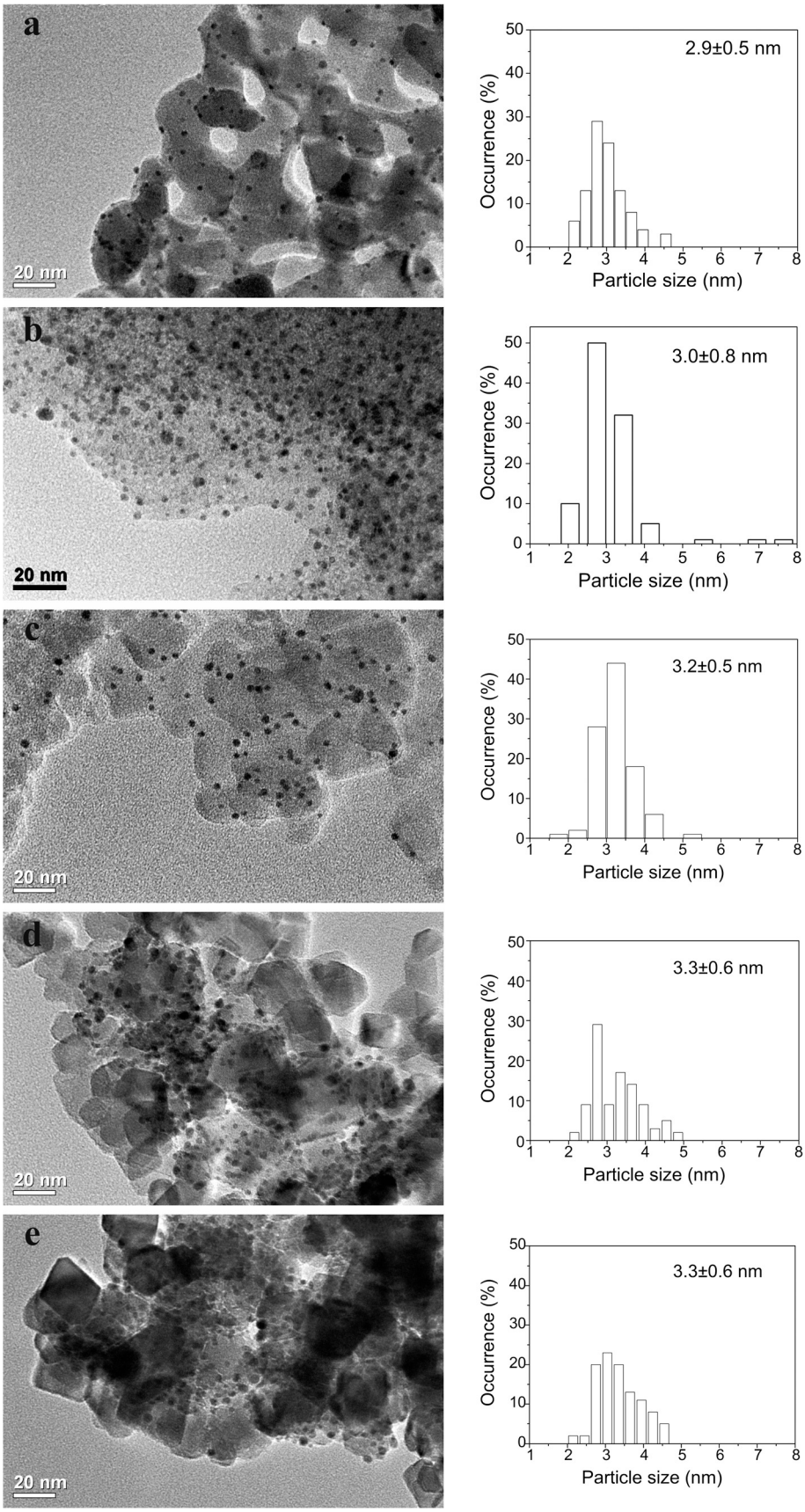

Fig. 3 TEM micrographs and the corresponding Au particle size distributions for fresh Au catalysts: a) Au(2.9)/ZnO; b) Au/Al_2O_3; c) Au/SiO_2; d) Au/TiO_2; e) Au/CeO_2.

Table 4 Surface content and relative surface distribution of gold species in Au catalysts

Catalysts	Au_{surf}[a] (%)	B.E. of $Au_{4f7/2}$ (eV)	FWHM (eV)	Au species (%)
Au(2.9)/ZnO	15.5	83.5	1.16	Au^0 (100)
Au/ZnO-300	11.4	83.4	1.19	Au^0 (100)
Au/Al_2O_3	11.0	84.7	2.21	$Au^{\delta+}$ (72.5)
		85.7	1.63	Au^+ (27.5)
Au/SiO_2	3.9	84.3	2.31	Au^0 (100)
Au/TiO_2	3.7	83.5	1.23	Au^0 (100)
Au/CeO_2	13.7	84.0	1.64	Au^0 (57.6)
		87.7	1.51	Au^{3+} (42.4)

[a] The surface gold weight content is calculated from the ratio of Au/M_xO_y obtained from the surface analysis by XPS.

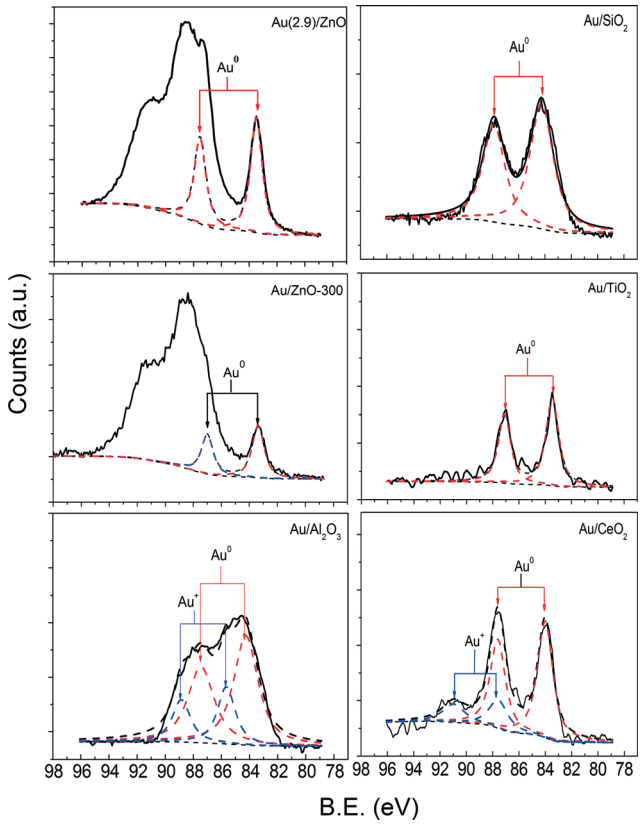

Fig. 4 Au 4f XPS spectra of the supported Au catalysts.

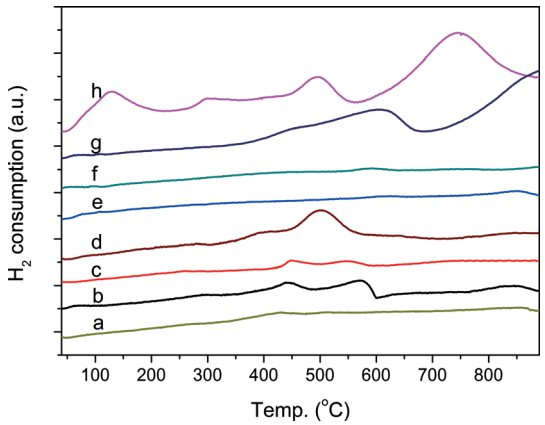

Fig. 5 H_2-TPR curves of Au catalysts and supports: a) ZnO; b) Au(2.9)/ZnO; c) Au/ZnO-300; d) Au/Al_2O_3; e) Au/SiO_2; f) Au/TiO_2; g) CeO_2; h) Au/CeO_2.

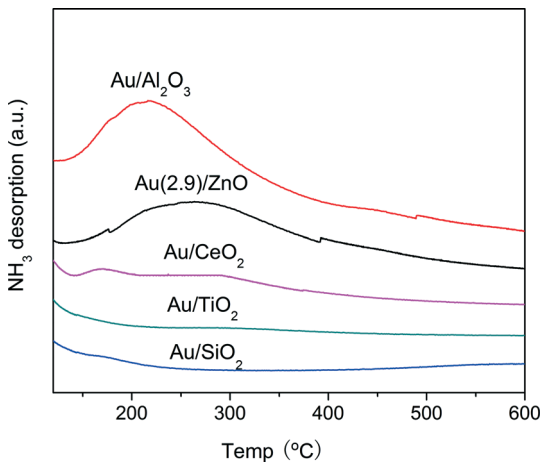

Fig. 6 NH_3-TPD spectra of the supported Au catalysts.

roughly independent of the diameter of the Au particles in the range of 2.9–7.4 nm. This fact is verified in both Au/ZnO and Au/Al_2O_3 catalysts and independent of the support. Previously, Comotti *et al.* also found that the catalytic activity of Au nanoparticles during glucose oxidation was inversely proportional to the diameter of the Au particles in the range of 3–6 nm,[33] which means that the catalytic activity per surface Au atom is independent of the diameter of the Au particles. Our present result is consistent with the result reported by Comotti *et al.*, and this observed correlation between activity and diameter agrees with the assertion that only exposed atoms are catalytically active.[34] However, for a Au mean particle diameter of around 2.0 nm, we found that both Au/ZnO and Au/Al_2O_3 had lower activities than those of around 3.0 nm Au.

It has been reported that a metal-to-insulator transition occurs as the particle size falls below 3.5 nm in diameter.[20,41,42] When the mean diameter of the Au particles is around 2 nm, the electronic properties are thus closer to that of insulator Au than bulk Au because of the quantum size effect. Hence, variations in the overall electronic properties of

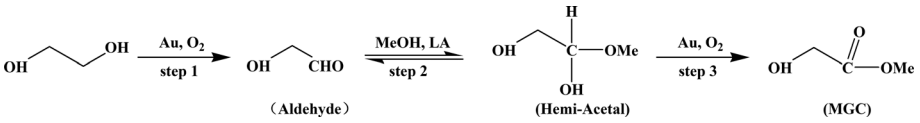

Scheme 1

the Au particles could be responsible for the lower activity of Au/ZnO with ~2.0 nm Au particles compared to that with ~2.9 nm Au particles. In fact, the low-temperature oxidation of CO on supported Au particles also shows a marked decrease in the turnover frequency (TOF, reaction rate per surface Au site per second) as the diameter of the Au particles is reduced to less than ~3 nm.[18,43]

On the other hand, the support also plays important roles in the oxidative esterification of ethylene glycol. The investigation of five Au catalysts, *i.e.* Au(2.9)/ZnO, Au/Al_2O_3, Au/SiO_2, Au/TiO_2, and Au/CeO_2, with similar Au mean particle diameters and Au loadings show that Au(2.9)/ZnO has the highest activity followed by Au/Al_2O_3, Au/SiO_2, Au/TiO_2, and Au/CeO_2.

From the characterization of these catalysts using TEM, XPS, H_2-TPR and NH_3-TPD, we believe that the main reason that Au/ZnO exhibits the highest catalytic activity can be explained as follows: first, ZnO has the strongest anchoring effect toward metallic Au particles. TEM confirmed that after the reaction the diameter of the Au particles in Au/ZnO increased slightly from 2.9 to 3.0 nm. Although Al_2O_3 also anchors Au particles well, around 27.5% of the Au in Au/Al_2O_3 is in the oxidized state, which is inactive in this reaction. The other supports, *i.e.* SiO_2, TiO_2 and CeO_2, have a far poorer anchoring effect toward Au particles. Second, the strong interaction between Au and ZnO increases the mobility of oxygen and lattice oxygen accessibility and this may promote the oxidative esterification reaction because it is generally considered that lattice oxygen plays an important role in alcohol oxidation, and the reaction undergoes the Mars–van Krevelen process.[44] Third, the acidity of ZnO may also play an important role in the oxidative esterification of ethylene glycol.

It is generally believed that the oxidative esterification of primary alcohols to methyl esters in the presence of gold catalysts involves three steps (see Scheme 1): first, the selective oxidation of primary alcohols in the presence of gold catalysts results in the formation of an aldehyde *via* the abstraction of β-H from the alcohol. A condensation reaction then occurs between the aldehyde and the alcohol leading to the formation of a hemiacetal species (step 2). Ester products are formed by the direct oxidation of hemiacetals (step 3).[7–12,45]

It has been reported that inorganic oxides contain appropriate acid sites that are able to facilitate hemiacetal formation and thus promote the formation of esters.[46] Previously, Su *et al.* also found that cooperation between Au nanoparticles and an acidic β-Ga_2O_3 support efficiently promoted the generation and subsequent oxidation of intermediates to the corresponding esters.[8]

5. Conclusion

We prepared three series of supported Au catalysts, namely, ZnO and Al_2O_3 supported Au nanoparticles with controlled mean diameters that range between 2.0 and 7.4 nm, and Au nanoparticles with uniform mean diameters (2.9–3.3 nm) that were loaded onto various supports. These catalysts were evaluated for the oxidative esterification of ethylene glycol to methyl glycolate. The results show that the catalytic activity per surface Au atom is roughly independent of the diameter of the Au particles in the range of 3–7.4 nm, whereas smaller Au particles (~2.0 nm) have inferior activity. This behavior was observed on both Au/ZnO and Au/Al_2O_3 catalysts. Au/ZnO with a mean Au particle diameter of ~2.9 nm could be reused at least three times without an obvious loss of activity. After storage in a refrigerator for 7 months, we obtained comparable catalytic activity to that of the fresh catalyst.

Among the five supported Au catalysts, Au/ZnO gave the best catalytic performance in the reaction followed by Au/Al_2O_3. Au/SiO_2, Au/TiO_2, and Au/CeO_2 gave far less catalytic activity. The high catalytic activity of Au/ZnO is likely due to the following: first, ZnO has the strongest anchoring effect toward metallic Au particles, which effectively suppresses the growth of Au particles during the reaction; second, the strong interaction between Au and ZnO increases the mobility of oxygen and lattice oxygen accessibility, which may promote the oxidative esterification reaction; third, cooperation between Au nanoparticles and the acidic ZnO support efficiently promotes the generation and subsequent oxidation of intermediates to the corresponding esters.

Acknowledgements

The authors gratefully acknowledge financial support from the National Natural Science Foundation of China (grant no. 20976101), the Program for Key Science and Technology Innovation Team of Shaanxi Province (2012KCT-21) and the Fundamental Research Funds for the Central Universities (GK201305011).

References

1 I. S. Nielsen, E. Taarning, K. Egeblad, R. Madsen and C. H. Christensen, *Catal. Lett.*, 2007, **116**, 35–40.
2 K. Ishihara, M. Kubota, H. Kurihara and H. Yamamoto, *J. Am. Chem. Soc.*, 1995, **117**, 4413–4414.
3 G. W. Breton, *J. Org. Chem.*, 1997, **62**, 8952–8954.
4 N. Mori and H. Togo, *Tetrahedron*, 2005, **61**, 5915–5925.

5 N. N. Karade, G. B. Tiwari and D. B. Huple, *Synlett*, 2005, **13**, 2039–2042.
6 C. E. McDonald, L. E. Nice, A. W. Shaw and N. B. Nestor, *Tetrahedron Lett.*, 1993, **34**, 2741–2744.
7 T. Hayashi, T. Inagaki, N. Itayama and H. Baba, *Catal. Today*, 2006, **117**, 210–213.
8 F.-Z. Su, J. Ni, H. Sun, Y. Cao, H.-Y. He and K.-N. Fan, *Chem. – Eur. J.*, 2008, **14**, 7131–7135.
9 E. Taarning, A. T. Madsen, J. M. Marchetti, K. Egeblad and C. H. Christensen, *Green Chem.*, 2008, **10**, 408–414.
10 B. Jørgensen, S. E. Christiansen, M. L. D. Thomsen and C. H. Christensen, *J. Catal.*, 2007, **251**, 332–337.
11 G. Liu, G. Li and H. Song, *Catal. Lett.*, 2009, **128**, 493–501.
12 G. L. Brett, P. J. Miedziak, N. Dimitratos, J. A. Lopez-Sanchez, N. F. Dummer, R. Tiruvalam, C. J. Kiely, D. W. Knight, S. H. Taylor, D. J. Morgan, A. F. Carley and G. J. Hutchings, *Catal. Sci. Technol.*, 2012, **2**, 97–104.
13 R. K. P. Purushothaman, J. van Haveren, D. S. van Es, I. Melian-Cabrera and H. J. Heeeres, *Green Chem.*, 2012, **14**, 2031–2037.
14 K. Suzuki, T. Yamaguchi, K. Matsushita, C. Iitsuka, J. Miura, T. Akaogi and H. Ishida, *ACS Catal.*, 2013, **3**, 1845–1849.
15 A. S. K. Hashmi and G. J. Hutchings, *Angew. Chem., Int. Ed.*, 2006, **45**, 7896–7936.
16 D. I. Enache, J. K. Edwards, P. Landon, B. Solsona-Espriu, A. F. Carley, A. A. Herzing, M. Watanabe, C. J. Kiely, D. W. Knight and G. J. Hutchings, *Science*, 2006, **311**, 362–365.
17 A. K. Sinha, S. Seedlan, S. Tsubota and M. Haruta, *Angew. Chem., Int. Ed.*, 2004, **43**, 1546–1578.
18 M. Haruta, S. Tsubota, T. Kobayashi, H. Kageyama, M. J. Genet and B. Delmon, *J. Catal.*, 1993, **144**, 175–192.
19 M. M. Schubert, S. Hackenberg, A. C. van Veen, M. Muhler, V. Plzak and R. J. Beham, *J. Catal.*, 2001, **197**, 113–122.
20 M. S. Chen and D. W. Goodman, *Catal. Today*, 2006, **111**, 22–33.
21 M. Comotti, W.-C. Li, B. Spliethoff and F. Schüth, *J. Am. Chem. Soc.*, 2006, **128**, 917–924.
22 D. Widmann, Y. Liu, F. Schüth and R. J. Beham, *J. Catal.*, 2010, **276**, 292–305.
23 S. Ivanova, V. Pitchon, C. Petit and V. Caps, *ChemCatChem*, 2010, **2**, 556–563.
24 Y. Guan and E. J. M. Hensen, *Appl. Catal., A*, 2009, **361**, 49–56.
25 K.-Q. Sun, S.-W. Luo, N. Xu and B.-Q. Xu, *Catal. Lett.*, 2008, **124**, 238–242.
26 C. Bianchi, F. Porta, L. Prati and M. Rossi, *Top. Catal.*, 2000, **13**, 231–236.
27 P. Haider, B. Kimmerle, F. Krumerich, W. Kleist, J.-D. Grunwaldt and A. Baiker, *Catal. Lett.*, 2008, **125**, 169–176.
28 W. Fang, J. Chen, Q. Zhang, W. Deng and Y. Wang, *Chem. – Eur. J.*, 2011, **17**, 1247–1256.
29 J. Strunk, K. Kähler, X. Xia, M. Comotti, F. Schüth, T. Reinecke and M. Muhler, *Appl. Catal., A*, 2009, **359**, 121–128.
30 M. B. Boucher, N. Yi, F. Gittleson, B. Zugic, H. Saltsburg and M. Flytzani-Stephanopoulos, *J. Phys. Chem. C*, 2011, **115**, 1261–1268.
31 N. S. Phala, G. Klatt, E. van Steen, S. A. French, A. A. Sokol and C. R. A. Catlow, *Phys. Chem. Chem. Phys.*, 2005, **7**, 2440–2445.
32 P. Bera and J. M. Vohs, *J. Phys. Chem. C*, 2007, **111**, 7049–7057.
33 M. Comotti, C. D. Pina, R. Matarrese and M. Rossi, *Angew. Chem., Int. Ed.*, 2004, **43**, 5812–5815.
34 H. Tsunoyama, H. Sakurai, Y. Negishi and T. Tsukuda, *J. Am. Chem. Soc.*, 2005, **127**, 9374–9375.
35 H. Tsunoyama, H. Sakurai and T. Tsukuda, *Chem. Phys. Lett.*, 2006, **429**, 528–532.
36 T. Ishida, N. Kinoshita, H. Okatsu, T. Akita, T. Takei and M. Haruta, *Angew. Chem., Int. Ed.*, 2008, **47**, 9265–9268.
37 S. Biella, F. Porta, L. Prati and M. Rossi, *Catal. Lett.*, 2003, **90**, 23–29.
38 M. Comotti, C. Pina, R. Matarrese, M. Rossi and A. Siani, *Appl. Catal., A*, 2005, **291**, 204–209.
39 J. Strunk, K. Kähler, X. Xia, M. Comotti, F. Schüth, T. Reinecke and M. Muhler, *Appl. Catal., A*, 2009, **359**, 121–128.
40 G. Jacobs, P. M. Patterson, L. Williams, D. Sparks and B. H. Davis, *Appl. Catal., A*, 2004, **258**, 203–214.
41 M. Valden, X. Lai and D. W. Goodman, *Science*, 1998, **281**, 1647–1650.
42 D. W. Goodman, *Catal. Lett.*, 2005, **99**, 1–4.
43 G. R. Bamwenda, S. Tsubota, T. Nakamura and M. Haruta, *Catal. Lett.*, 1997, **44**, 83–87.
44 J. Huang, W.-L. Dai and K. Fan, *J. Catal.*, 2009, **266**, 228–235.
45 A. Abad, P. Concepcion, A. Corma and H. Garcia, *Angew. Chem., Int. Ed.*, 2005, **44**, 4066–4068.
46 D. I. Enache, D. W. Knight and G. J. Hutchings, *Catal. Lett.*, 2005, **103**, 43–52.

